JOINT EUROPEAN TORUS

JET–P(91)52

H. Fajemirokun, C Gowers, K Hirsch,T Kajiwara, P. Nielsen,
H. Salzmann and JET Team

High Resolution LIDAR Thomson Scattering at JET

High Resolution LIDAR Thomson Scattering at JET

H. Fajemirokun[1], C. Gowers, K. Hirsch[2], T. Kajiwara[3,4], P. Nielsen,
H. Salzmann and JET Team*

JET-Joint Undertaking, Culham Science Centre, OX14 3DB, Abingdon, UK

[1]Imperial College of Science, Technology and Medicine, London, UK
[2]Institute F. Plasmaforschung, Universitiit Stuttgart, 7-Stuttgart
[3]Interdisciplinary Grad. School of Engineering Sciences, Kyushu University, Japan
[4]Max-Planck-Institut für Plasmaphysik, Garching, FRG
** See Appendix 1*

Preprint of Paper to be submitted for publication in
IoP

ABSTRACT.

A high resolution LIDAR Thomson scattering system for JET has been designed, using a streak camera detection system. The best achievable spatial resolution of the existing LIDAR system is 9–l0cm. There is a need for higher resolution than is presently achievable in order to resolve the density and pressure gradients at the plasma edge during H-mode operation of JET. An additional motivation is the possibility of taking high resolution LIDAR snapshots of islands in the core of the plasma. It has been reported that by using a streak camera system, resolution of better than 4cm is in principal possible, over a limited part of the plasma radius. Some feasibility experiments were carried out during a portion of the last JET period of operations (1:9:90–3:11:90). A Hadland 675 Imacon streak camera and 50/40 intensifier formed the detection system, and a Tektronix DCS digitizing CCD camera system recorded the data and transferred it to a PC for analysis. Results obtained on the stray light signature, plasma light levels and our initial attempts to record scattering results are reported here. In addition, some general problems encountered in the operation of the detection system and the interpretation of data are discussed. Using a Thomson CSF streak camera, intensifier and digitizing CCD camera system, and a set of optimized high filters, a system to make high resolution electron temperature and density measurements has been constructed and calibrated.

i) Introduction

The LIDAR-Thomson Scattering diagnostic, has been operating successfully at JET since July 1987. Originally, the best achievable spatial resolution was around 12 cm. This figure is determined by the pulse width of the laser, τ_L, and the response time of the detection system, τ_D, according to the relation (assuming gaussian laser pulse and detector response);

$$\delta L = \frac{c(\tau_L^2 + \tau_D^2)^{1/2}}{2} \qquad (1)$$

where c is the speed of light. Latterly, this figure has been improved to around 9-10cm, by deconvoluting the received signal from the total response function of the system (the Green's function of the system). Using the existing system, it seems unlikely that any further improvements in spatial resolution will be possible across the whole profile. However, it would be of interest to resolve locally distances significantly smaller than this figure at the edge of the plasma, because in H-mode operation the scale lengths of the electron density gradient, the electron temperature gradient and the electron pressure gradient are less than 9 cm (fig.1). Understanding the nature of these gradients would yield important information on ballooning and other modes in the plasma. To attain better spatial resolution with a LIDAR system requires a detection system with a faster response time than the microchannelplate photomultipliers and transient digitizers presently used, which have a combined bandwidth of 700 MHz. In addition, any shortening of the laser pulse would clearly be helpful.

Large improvements in the detector response time may be realised by switching to a streak camera detection system. Streak cameras with a streak speed of up to 30 ps/mm are available on the market. The pulse length of the ruby laser currently in use on the LIDAR-Thomson scattering diagnostic may be reduced to 180 ps by the addition of an appropriate mode-selecting etalon in the laser oscillator cavity. At this pulse length, the laser energy per pulse is around 2J.

The system considered here (schematic, fig.2) shares the existing LIDAR-Thomson scattering system laser and input optics, but only uses one of the six beams of collected light from the output collecting mirror array (the remainder of the array will continue to be used by the existing LIDAR-Thomson scattering system). A three channel filter spectrometer divides the light into three frequency bands before it is focused down into 3 spots on the streak camera photocathode by a fast F/1 lens. A CCD camera records the output of the streak camera image intensifier and the data is stored in digitised form on a personal computer. It will be shown that spatial resolution of less than 4 cm is achievable using such a set-up. Even better resolution could possibly be obtained by using a deconvolution technique on the observed data, similar to that used on the present LIDAR-Thomson scattering system and this is also being investigated.

ii) Modus operandi

A basic description of the LIDAR-Thomson scattering concept is given in [1]. Collected Thomson scattered light passes through a 3-channel spectrometer and thence via an F/1 focusing lens to the streak camera photocathode. The streak image will consist of three parallel lines, side by side, which vary in intensity along their length. By fitting a spectrum to the 3 channel intensity distribution at each temporal resolution element on the streak camera record the electron temperature and density profile for a 0.5 m long radial section of plasma can be deduced. For a given focused spot size, X, on the photocathode and a given sweep speed, S, the temporal resolution (i.e.response time of the detector) of the streak camera is just XS. For example, a sweep speed of 75 ps per mm (well within the capability of available cameras) and a spot diameter of 2mm yields a temporal resolution of just 150 ps. Inserting this into the formula for the spatial resolution and taking a laser pulse time of 180 ps yields a minimum resolvable length inside the plasma of 3.5 cm.

iii) Collection optics

The backscattered light from the plasma first passes through a quartz output window of diameter 17 cm whose centre is displaced 19 cm vertically from the mid-plane of the torus. The light is then focused by a single spherical mirror of diameter 35 cm and focal length 2 m, such that a point at a major radius of 3.9 m is imaged close to a small newtonian mirror. The spherical mirror has an effective solid angle of collection of 1.2×10^{-3}sr. In turn, the newtonian mirror is imaged onto a field lens in the roof of the torus hall by a second spherical mirror of diameter 30 cm and focal length 2.00 m . After passing through a two mirror labyrinth, the plasma is finally imaged by an achromatic doublet, which is placed in the image plane of the second spherical mirror. It is at this point that the scattered light for the high resolution LIDAR system is separated from that of the existing LIDAR system. A 1:1 image of the plasma is formed about 1m from the achromat, after passing through an aspheric corrector plate and a thin (focal length 1 m) compensating lens. The compensating lens is necessary because the focal length of the first spherical mirror is optimised for the original LIDAR system, i.e. to image the centre of the plasma (at major radius 3.05 m), not the edge.

iv) Spectrometer design

A number of constraints determine the nature of the spectrometer to be used in the system. Most importantly, the number of photons collected by the collection optics from a single spatially resolved element in the plasma must be considered. The length of a spatially resolved element is about 3.5 cm as calculated above. The number of photons, n_{pe}, scattered from this plasma element and delivered by the collection optics to the streak camera photocathode is given by the formula

$$n_{pe} = n_e n_{pi} (\sigma_e / A) V \Omega T \qquad (2)$$

where n_e is the electron density in the plasma, n_{pi} is the number of incident photons, σ_e is the classical electron cross-section, A is the cross-sectional area of the incident laser beam, V is the scattering volume, T is the total optical transmission and Ω is the solid angle subtended by the collecting mirror (note $V/A = \delta L$, the resolution element length). For collection optics as described above with a total transmission of 20%, a laser energy of 2J at 694 nm and an electron density of $10^{19} m^{-3}$, n_{pe} = 4800. For an S25 photocathode, the quantum efficiency at 694 nm is about 3%. Therefore the number of photoelectrons produced per resolution element would typically be 144; not a very large number, but certainly detectable. The paucity of photoelectrons means that a diffraction grating spectrometer is unfeasible, as this would spread the photons over a whole spectral range. It is more promising to use an edge or bandpass filter spectrometer, which splits the incoming light into a small number of spectral bands and concentrates this light at points on the photocathode. The overall transmission of such a system is also typically higher by a factor 1.5. Two channels are required to determine the electron temperature, but using only two channels precludes performing the kind of statistical analysis on the data as described in [2]. Therefore a three channel filter spectrometer is favoured. Having specified a three channel system, it is necessary to determine the optimum frequency ranges of the channels for the required dynamic range in electron temperature, i.e. .01 - 1.5 keV. Using a simulation code good frequency bands for the system were found to be; 500nm to 580nm, 580nm to 675nm and 675-690 nm.

Before the light reaches the streak camera, stray laser light and plasma light must be extracted from the collected light. This is most efficiently done by using a sharp-edged bandpass filter in each channel, positioned after the edge channel filters, to reject unwanted light.

Finally, the optical path followed by light in each of the three channels must follow the same optical path to within 1 cm (less than 1 resolution element) to best use the whole available streak length and avoid an extra consideration in the time calibration of the system.

After the light passes through the spectrometer the 3 plasma images must be demagnified into as small a spot as possible on the streak camera photocathode. For a 2mm diameter spot on the photocathode an F/1 final focusing lens is required, if the scattering volume diameter in the plasma (i.e. the laser beam diameter) is 4cm.

v) Specification of streak camera.

The first consideration in the streak camera specification is to choose an appropriate streak rate. Taking into account eqn(1), it is clear that little is to be gained in terms of spatial resolution by having a streak camera response time of much less than the laser pulse time (180 ps). A streak camera response of 150 ps is reasonable, and for a 2mm light spot on the photocathode (achievable by using F/1 optics), this equates

to a streak rate of 75 ps/mm. In order to observe 0.5 m of plasma at this streak rate, a 45 mm streak length is necessary (assuming 1:1 magnification in the streak camera tube).

Both before and after the arrival at the streak camera of scattered light from the edge plasma region, a large pulse of stray laser light arrives (around 10^6 times larger than the scattered light signal), the first from the torus input window, the second from the torus inner wall. This dictates that the on/off gating ratio of the streak camera should be $> 10^6$. The laser light from the observed 0.5 m region arrives over a period of 3.3 ns and the total laser flight time to the inner wall and back is around 14 ns. A gating rise/fall-time for the streak camera of less than 10 ns is therefore required, with a post gate suppression period of typically 100 ns.

vi) Experimental Aims.

From the discussion and experimental work described thus far, it is clear that in order to make high resolution LIDAR-Thomson scattering measurements at the plasma edge, a custom built streak camera and tightly specified bandpass and edge filters are required. However, having already set up much of the optical system, it has been possible to obtain valuble experimental data before these special components became available by using a loaned streak camera and a set of (un-optimized) filters.

a) to characterize stray laser light pulses;

b) to gain experience in the details of the experimental set-up (eg. triggering schedules);

c) to attempt to observe Thomson scattered light from high density plasmas;

d) to develop and test analysis software on real signals;

During the last two months of the JET operational period running from 29:8:90 to 3:11:90, the Hadland 675 Imacon streak camera and accompanying intensifier unit previously used in preliminary experiments described in [1], were available. It was therefore proposed to use this equipment, in conjunction with a set of blocked bandpass filters designed to reject ruby laser light but with pass-bands fairly close to and on the short wavelength side of the laser line, in an attempt to make some relevant observations. The edge filter/mirror stack shown in the schematic was replaced simply by a mirror, so all measurements made were 1-channel measurements. Later during the experimental period, a notch filter which transmitted ruby laser light (about 99% transmission at 694.3nm) but strongly rejected the remainder of the visible spectrum became available and was used in place of this mirror.

vii) Expected Plasma Light Level.

A mention must be made of the signal expected to be detected by the system due to plasma light since this is a potential source of noise. In the plasma, conditions are such that bremsstrahlung, recombination and line radiation all make important contributions to the plasma light in the spectral region of interest. However, a calculation of the order of magnitude of the bremsstrahlung contribution will serve to illustrate a comparison of the order of magnitude of background signal due to plasma light with the scattered light signal. For a plasma with Z_{eff} approaching unity, the number of photons radiated by bremsstrahlung in wavelength band $d\lambda$ (nm) is given by [3],

$$n_p = 7.62 \times 10^{-21} \; (n_e^2/\lambda T_e^{1/2}) \, G_{ff} \Omega \tau V_p \; d\lambda \qquad (3)$$

where n_e is the electron density (m^{-3}), T_e is the electron temperature in eV, G_{ff} is the free-free Gaunt factor, Ω is the solid angle subtended by the optical collection aperture (10^{-3}sr), τ is the integration time (14ns) and V_p is the portion of the radiating plasma volume accessible to our optical system (2.0x0.0012 m^3). For a JET plasma with a line average electron temperature of 3000 eV, electron density $2x10^{19} m^{-3}$ and a G_{ff} of 3, this yields 90 photons in a bandwidth of 10nm centred at 640nm. It is usual practice (e.g [3]) to multiply the pure hydrogen bremsstrahlung estimate by a factor of 100 to give a worst case scenario for plasma background (bremsstrahlung + line + recombination contributions) in a tokamak, giving a total plasma light estimate of 9000 photons.

Comparing this figure with the total number of scattered photons expected in the same wavelength interval (integrating over a 2m scattering length because using a slow streak rate, scattered light from the whole plasma may in principal be collected), of about 91,000 yields a signal to worst case plasma light ratio of better than 10. Therefore, the plasma light background source was not expected to be a problem in this experiment.

The actual signal to noise ratio (i.e., the relative size of quantum noise fluctuations in the signal) is obtained by comparing the number of signal quanta to the square root of the sum of the number of signal quanta plus plasma light quanta (since quantum statistics dictates that the noise fluctuation is the square root of the total signal; any non-fluctuating background level may simply be subtracted). This calculation should be performed at the point in the detection system where the respective number of quanta are smallest, and this is in the streak camera, after the signal has been photoelectrically converted to electrons at the photocathode but before amplification in the intensifier. The quantum efficiency of an S20 photocathode at 640nm is around 2%, and using this figure in the calculation yields a signal to noise ratio of better than 40. Thus, quantum noise considerations may be neglected

viii) Set-up and Description of Apparatus.

a) Optics

A photograph of the experimental set-up is shown, figs.3. The emphasis here is on the mechanical details of the actual set-up used, though changes to the optical design described earlier are noted and discussed.

Light collected and focused by the vertical spherical mirror array in the torus hall is transferred to the roof laboratory via a relay optical system. The beam from the upper spherical mirror is separated from the remainder of the light at an image plane of the vertical spherical mirror array. The bulk of the collected light goes to the original LIDAR-Thomson scattering microchannelplate photomultiplier detectors. The beam separation is performed by an elliptical plane mirror placed in the path of the beam from the upper spherical mirror at 45° to the beam, supported by a hollow finger assembly which is bolted onto a metal mask in front of the achromatic lens (an image plane of the vertical mirror). The light is redirected through an f = 0.5m field lens (for the plasma image) by another small mirror held by an adjustable assembly screwed into the edge of the light box.

At the next image plane of the vertical mirror is placed an f = 1m lens, just behind which is a plane mirror which directs the light from the plasma back through the f = 1m lens and (via another plane mirror) to a f = 0.5m field lens. This field lens is in turn imaged by an aspheric demagnifying lens working at focal ratio F/0.9 onto the photocathode of the streak camera. Thus, an image of the scattering plasma volume is formed at the streak camera photocathode.

As described, the optics will image the centre of the plasma in the JET vessel, at a major radius of 3.05m. However, since the diagnostic in its final form will be primarily intended to make measurements at the plasma edge, a thin (f =0.8m) corrector lens may be inserted at the base of the elliptical mirror support finger, very close to the achromatic lens. This has the effect of modifying the optics in the roof lab to be a relay system for, and to image at the photocathode, light from a major radius of 3.9m, the plasma edge region.

The aspheric demagnifying lens must be mounted very close to (around 2 cm) the streak camera photocathode. To allow this, the shutter assembly in front of the photocathode was removed and a custom made lensholder fixed in place, utilising the shutter assembly screw holes. So that the shutter could still be used if required, the lensholder was made with screw holes allowing the shutter assembly to be affixed in front of the lens.

The optics in the roof laboratory up to and including the first f=0.5m lens are enclosed in the original LIDAR light-tight box. The remainder of the optics are enclosed by specially built light boxes, designed to be easily removable to facilitate adjustments to the optics in between JET plasma pulses. A heavy black cloth was used as a light seal around the camera aperture.

b) Detection system

The streak camera used throughout these experiments was a Hadland 675 Imacon model obtained courtesy of Imperial College, London. The photocathode fitted is a glass fronted S20. The streak rate of this camera is adjustable over the range from 10nsmm^{-1} down to 30 psmm^{-1}, and during the course of the investigations the streak rates 1nsmm^{-1}, 2nsmm^{-1} and 5nsmm^{-1} were utilized. The magnification of the electron optics inside the streak tube was set at x3 throughout, so the actual streak rates observed at the output of the streak tube for the settings used are 1/3nsmm^{-1}, 2/3nsmm^{-1} and 5/3nsmm^{-1} (i.e indicated rate divided by 3). After intensification and processing the scales on the A4 printouts become approximately 0.25, 0.5 and 1.4nsmm^{-1} respectively.

As the laser pulse moves through the plasma, the light collected by the collection optics in fact forms a moving image at the photocathode. The direction of the motion of the focused image is in the vertical plane. If the streak camera is oriented so that this image motion is in the direction of the streak, then the effect of this spot motion manifests itself as a small increase in the effective streak speed, which poses no major problem to the interpretation of results. If, however, the streak is perpendicular to this direction, the streaked image will no longer appear as a straight line, making analysis more difficult. In addition, for a multichannel system with two or more focused images squeezed onto the photocathode, a channel may be shifted beyond the edge of the photocathode. Therefore, the camera was mounted on its side, so that the streak direction is in a vertical plane.

A related issue is the defocusing of the laser pulse as it moves through the plasma. Any design of collection optics can only image one point in the plasma at the photocathode; other points are by definition out of focus to some degree. For a high resolution edge diagnostic which only examines perhaps 0.5m of plasma or less, this defocusing effect is unimportant. However, the defocusing of the spot is a fundamental barrier to obtaining high resolution measurements along the whole plasma radius using a single streak camera and collection optical system, because for much of the plasma chord the out-of-focus spot size will be large, causing the effective integration time of the streak camera to be long (of course, other fundamental problems exist in making such a measurement, such as the trade-off between spatial resolvability (a function of streak rate) and the available streak length of existing streak cameras). The depth of focus of the collection optics could always be improved by increasing the focal ratio of the collection aperture, but this means that less scattered light is collected. As the expected signal is already close to the limits of detectability, this is an undesirable course of action.

To trigger the detectors, the voltage pulse from a Pockel's cell, acting as a single pulse selector in the ruby laser system, was used.

ix) Results.

a) Initial results

The laser was fired at the JET plasma commencing on shot 22635 with the camera set to the 1ns/mm streak rate. The signals recorded consisted of two distinct components; i) sharp, intense peaks whose position on the streak record could be moved by adjusting the relative delay on the arrival of the trigger pulse at the camera and ii) a background of lower intensity but extending over the whole of the camera record and whose features appeared completely independent of the trigger timings (fig.4). The sharp peaks behaved in a manner consistent with the expected stray laser light pulses originating from reflections of the input laser beam. A schedule of expected stray light pulses was constructed and matched to what was observed in and around the time window of interest (fig.5).

Fig. 5 shows a streak camera record on the 5nsmm^{-1} streak rate, when the laser was fired into a vacuum. Only the first of the two components mentioned above is seen here. Identifiable stray light pulses are from the input window of the torus (observed via two different routes in the collection optics) and the torus inner

wall. Neither the input window nor the inner wall are imaged by the collection optics, and so these pulses appear out of focus on the streak camera photocathode giving relatively long duration signatures due to this blurring. In this case the filter in use had a pass band of 6nm centred at 683nm. Its transmission of ruby laser light was measured to be 2.9×10^{-3}.

Explanation of the background signal (e.g. fig. 4) posed more of a problem. The time independence (at least on a ns timescale) of this signal and its intensity variation with plasma density (no plasma, no background) are consistent with a plasma light signal. However, its observed absolute intensity at this streak speed was 3 orders of magnitude in excess of what might be expected for a worst case plasma. This could be explained if the post-streak gating of the camera was not working correctly. On a Hadland 675 camera, the post-streak gating is designed to operate in the following manner: a large (kV) "blanking-pulse" voltage is applied for 10ms to the high voltage focusing mesh just behind the photocathode of the streak camera in order to completely defocus the electron beam originating at the photocathode, effectively gating out any signal with a gating ratio of 10^7 . Thus, when about 30μs after the end of the streak, the sweep plates of the camera are reset to the starting position (an action which would sweep the beam slowly back across the phosphor screen were it not defocused), nothing is seen at the output of the streak camera. If this blanking pulse system were defective, and the flyback signal were visible, then the plasma light level would seem anomalously large because the flyback occurs over a period of around 50μs, 3 orders of magnitude slower than the streak.

Initial investigations into this effect, performed by illuminating the photocathode with a constant light source, showed that the signal recorded was roughly constant in intensity for a range of streak rates from $1 nsmm^{-1}$ down to $60 psmm^{-1}$, demonstrating that the recorded signal was to a large extent independent of the indicated streak rate. At slower streak speeds ($2 nsmm^{-1}$ and $5 nsmm^{-1}$) a smaller signal was observed, indicating that the observed effect was less severe in these regimes, a fact used in the quantitative experiments performed later on.

Attempts to shutter out the effect, using a liquid crystal shutter with a closing time of 200μs, failed. This result is commensurate with an un-gated flyback signature occurring on a shorter timescale than 200μs. Since the high voltage blanking pulse is switched by a krytron tube, which is mounted so as to be visible when the camera front panel is opened, its operation may be checked by i) seeing by eye if it fires and ii) seeing how soon it fires after the end of the streak using a photomultiplier. These tests indicated that the krytron fired 700ns after the end of the streak, i.e. it appeared to be operating at the correct time.

Experiments using a laser diode to characterise the detection system confirmed that the flyback signal was visible. Figure 6 shows a streak record of a laser diode producing 20ns pulses every 4μs. Only one such pulse could be recorded by the actual streak (due to the 4μs rep-rate) and in any case its intensity would be too low to be detectable. This recorded signal is, therefore, a flyback signature in the absence of a blanking pulse.

As stated above the problem was less severe at streak rates of $2 nsmm^{-1}$ and $5 nsmm^{-1}$, so these rates were used in attempts to observe scattered signal. In addition a set of filters were used to further attenuate plasma light signals and laser stray light pulses (one of which arrives very closely in time to the scattered signal from the plasma). The filters were mounted directly in front of the aspheric focusing lens on the front of the

camera. Laser stray light was further attenuated by use of a notch transmission filter in place of mirror 3.

b) scattering results

Using a bandpass filter centred at 640nm, along with the ruby laser notch transmission filter in place of mirror 3 in the figure, a reproducible feature was observed on the CCD record, just earlier than the inner wall stray light pulse. Measurements were made at $2nsmm^{-1}$ and $5nsmm^{-1}$ (figs 7, 8). The signal was not observed at times when there was no plasma or when the detection system was triggered without the laser having fired. The signal was always centred 8ns before the peak of the inner wall pulse, i.e. at a time corresponding to the arrival of Thomson scattered light from the plasma centre. In verifying this, a geometrical correction must be taken into account due to the motion of the image spot on the photocathode (arranged, as described earlier, to move parallel to the streak direction). This correction is independent of streak speed and was shown by the optical design software to correspond to the image of the centre of the plasma appearing 1cm further away from the inner wall pulse on the A4 record than would be expected from purely temporal considerations.

With the calibration data obtained in the laser diode experiments described in the next section, it is possible to approximate the number of photons corresponding to the signals of interest in figs.7, 8. This may then be compared to the expected number of photons calculated using the simulation program. Using the expression,

$$n_{ps} = \tau P \gamma \frac{\eta_{750}}{\eta_{640}} E_p \qquad (4)$$

where n_{ps} is the number of photons represented by the feature, P is the laser diode laser power required to produce a signal of the same magnitude, E_p is the energy per photon at 640nm, τ is the time duration of the signal, η is the quantum efficiency of the S20 photocathode at the subscripted wavelength and γ is the pincushion screen correction, yields the following results;

7a) $1.2 +/- 0.4 \times 10^5$ photons

7b) $1.1 +/- 0.4 \times 10^5$ photons

8) $1.4 +/- 0.5 \times 10^5$ photons

These numbers compare with an expected value of 0.8×10^5 for a typical JET plasma.

x) Conclusions.

a) Stray light

Measurements of both the timing and magnitude of stray light pulses observed in these experiments suggest that it will not be a problem in the forthcoming attempts to investigate the plasma edge region and magnetic island structures at high resolution. Even using a non-optimized filter set, it was possible to time resolve these signals without precipitating complete saturation or severe blooming of the streak camera photocathode. It should further be noted that the inner wall pulse was considerably larger than usual throughout this operational period because the inner wall tile on which the laser pulse usually dumps became detached during a disruption, allowing the laser beam to scatter from a shiny metal surface.

b) Scattered light signals

There is strong, though not conclusive, evidence that a Thomson scattered signal was detected. The feature in question was,

i) reproducible,
ii) only present when laser pulse and plasma present,
iii) of the expected magnitude,
iv) at the expected time.

c) Flyback and plasma light

The problems encountered with the streak camera gating system highlight the importance of the highly specified gating performance of the camera built for the high resolution system. The estimate of the magnitude of the plasma light signal yielded from the spurious flyback signal (around $x10^9$ enhanced) implies that in a correctly gated camera this should not be visible.

d) Triggering

The system was triggered reliably from the spare single pulse selector output of the laser.

xi) Present status (as of 1:7:91).

The system (described in the first five sections of this paper) designed to acquire high resolution data has been set up. Using a streak camera, intensifier and a digitising CCD camera system supplied by Thomson CSF and a set of high specification filters, high resolution observations of JET plasmas will be

attempted. It is intended to look both at the edge plasma region and to take high resolution snapshots of pellet induced snakes on the $q=1$ surface.

The calibration of the system is a three stage procedure. First, the spectral response of the system was measured, and is shown fig.(9). This measurement is performed by illuminating each channel with light from a grating spectrometer and measuring the output. Secondly, the relative sensitivity of the three channels is measured, using a calibrated blackbody source to illuminate the three channels. The source used is a circular target painted with TiO_2 illuminated by a tungsten lamp. Finally, the absolute sensitivity of the system is obtained by comparing recorded signals with corresponding density measurements from the main LIDAR Thomson scattering system.

References

[1] H. Fajemirokun et al. (1990), Rev Sci Instrum 61 (10) pp 2843

[2] H. Fajemirokun et al. (1990), Rev Sci Instrum 61 (10) pp 2849

[3] R. Prentice (1978), " The DITE Tokamak multi-purpose Thomson scattering system". CLM-R 179

Fig.1) JET H-mode density profile.

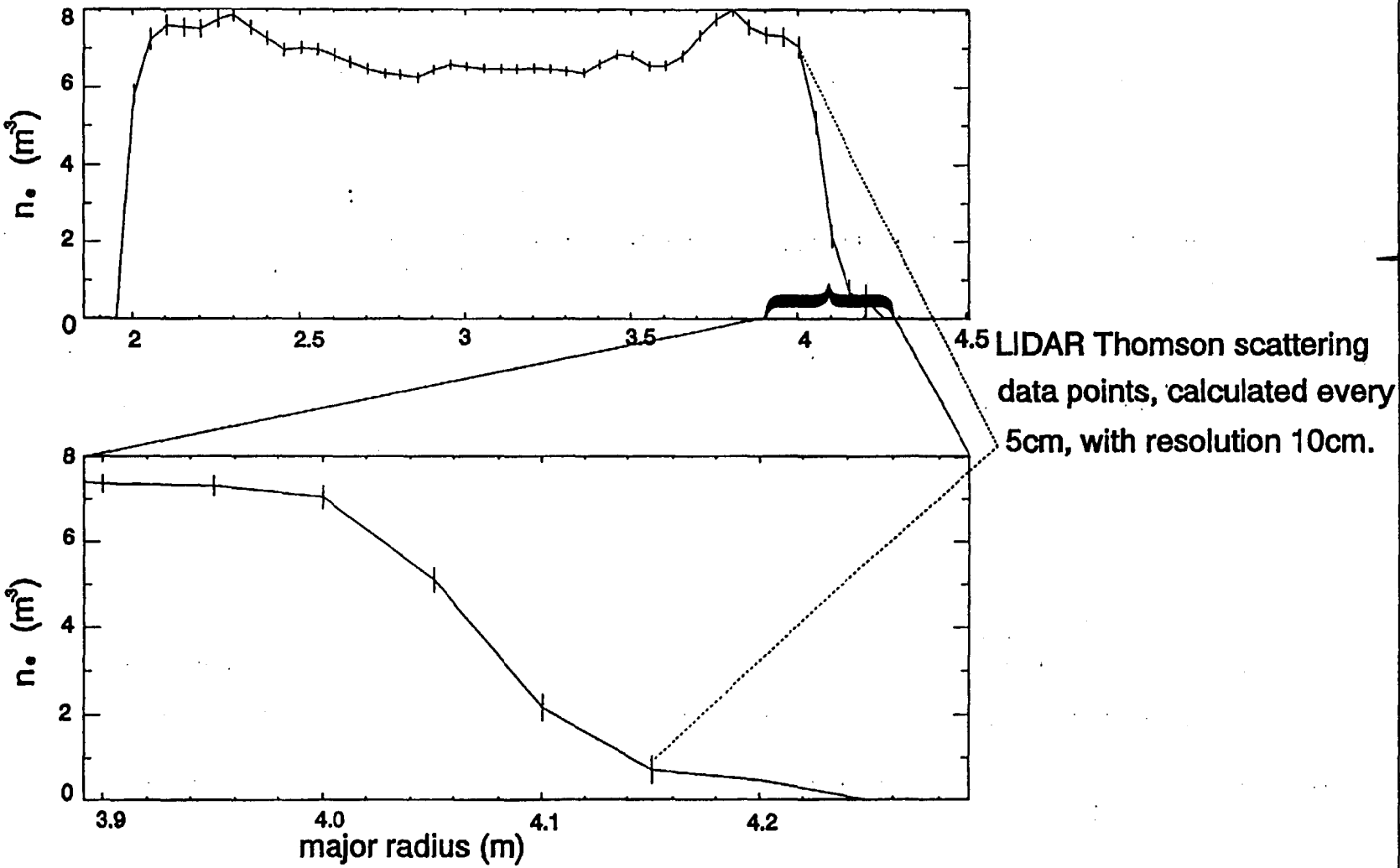

[1] H-mode edge density gradient

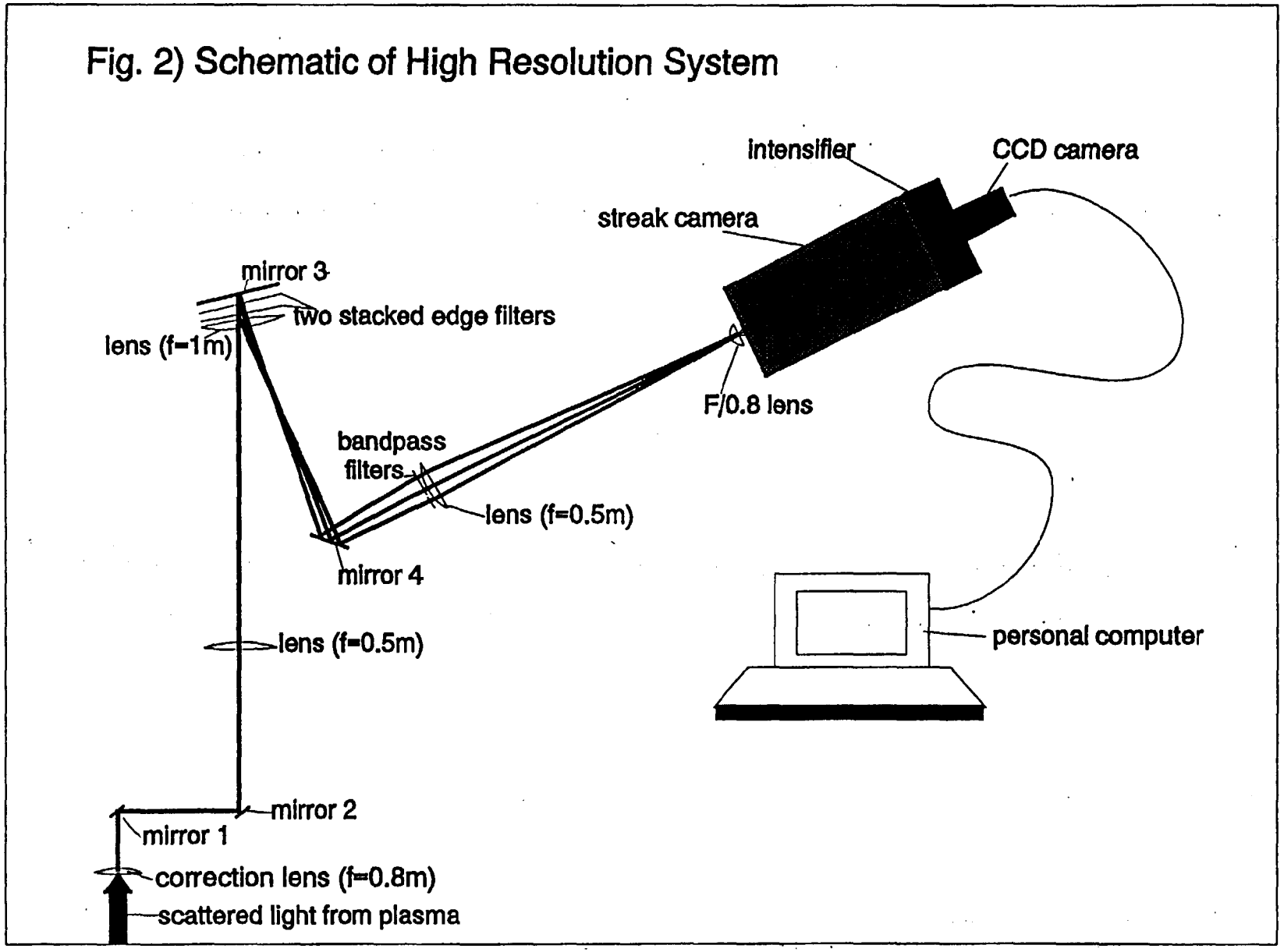

[2] Schematic of high-resolution system design

Fig. 6) Flyback

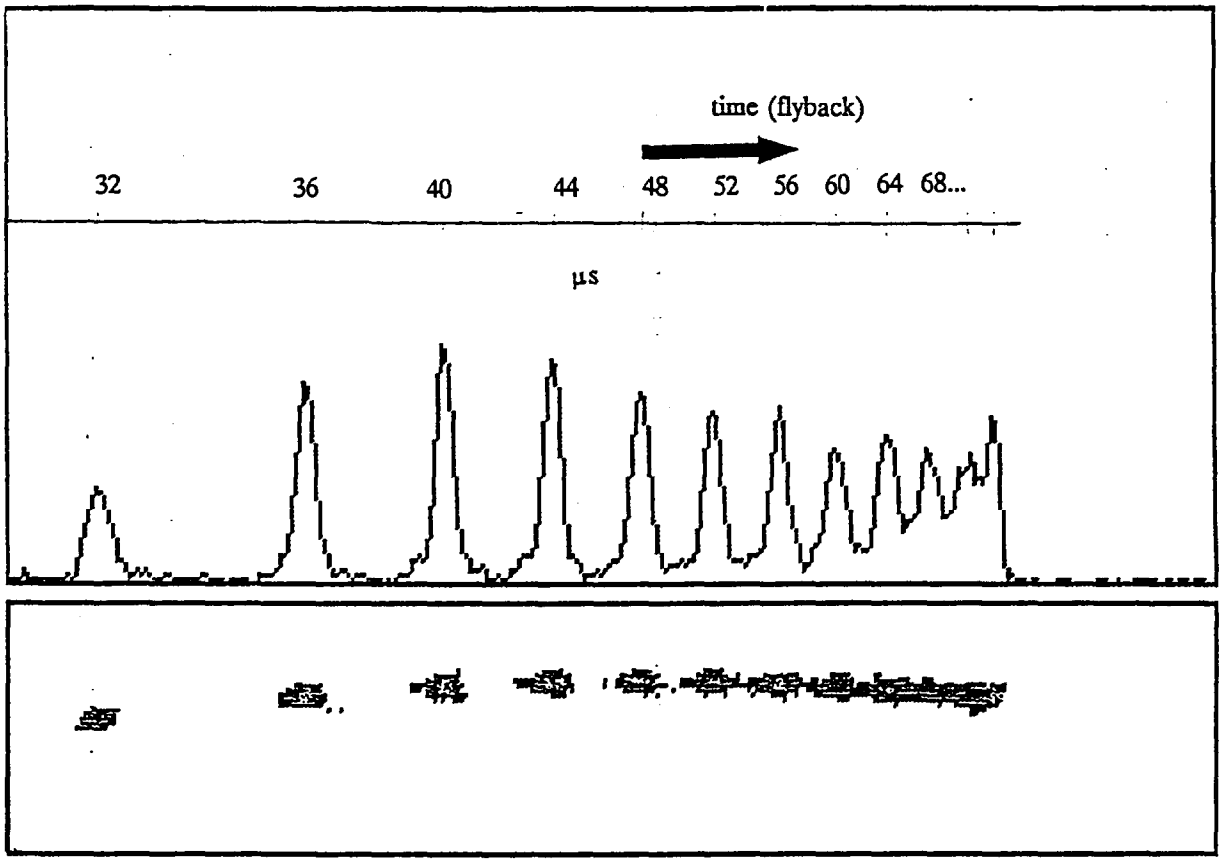

[6] Flyback signature characterized by laser diode

Fig. 7a) Detected Signal (5ns/mm)

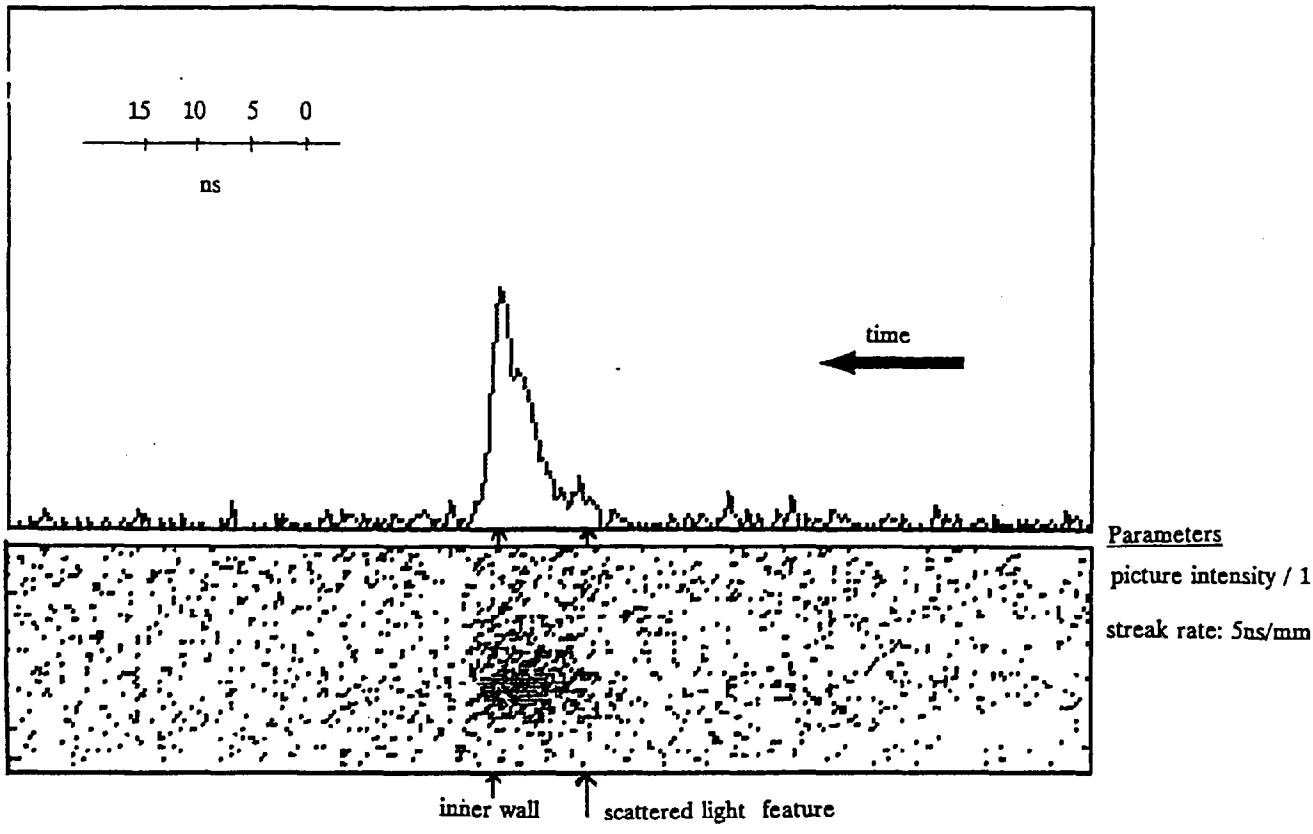

Fig. 7b) Detected Signal (5ns/mm)

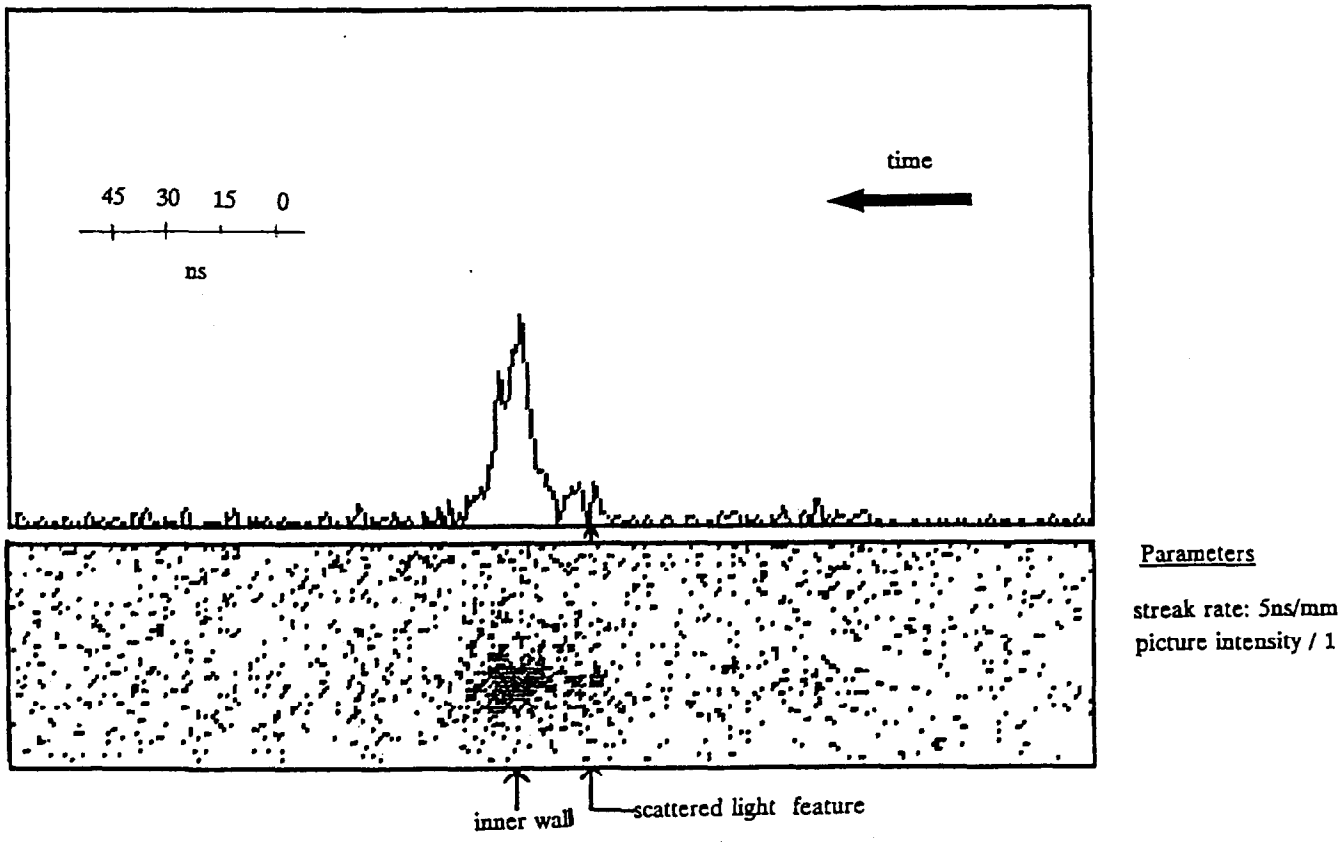

[7] Scattered signals - indicated streak rate 5ns/mm

Fig. 8) Detected Signal (2ns/mm)

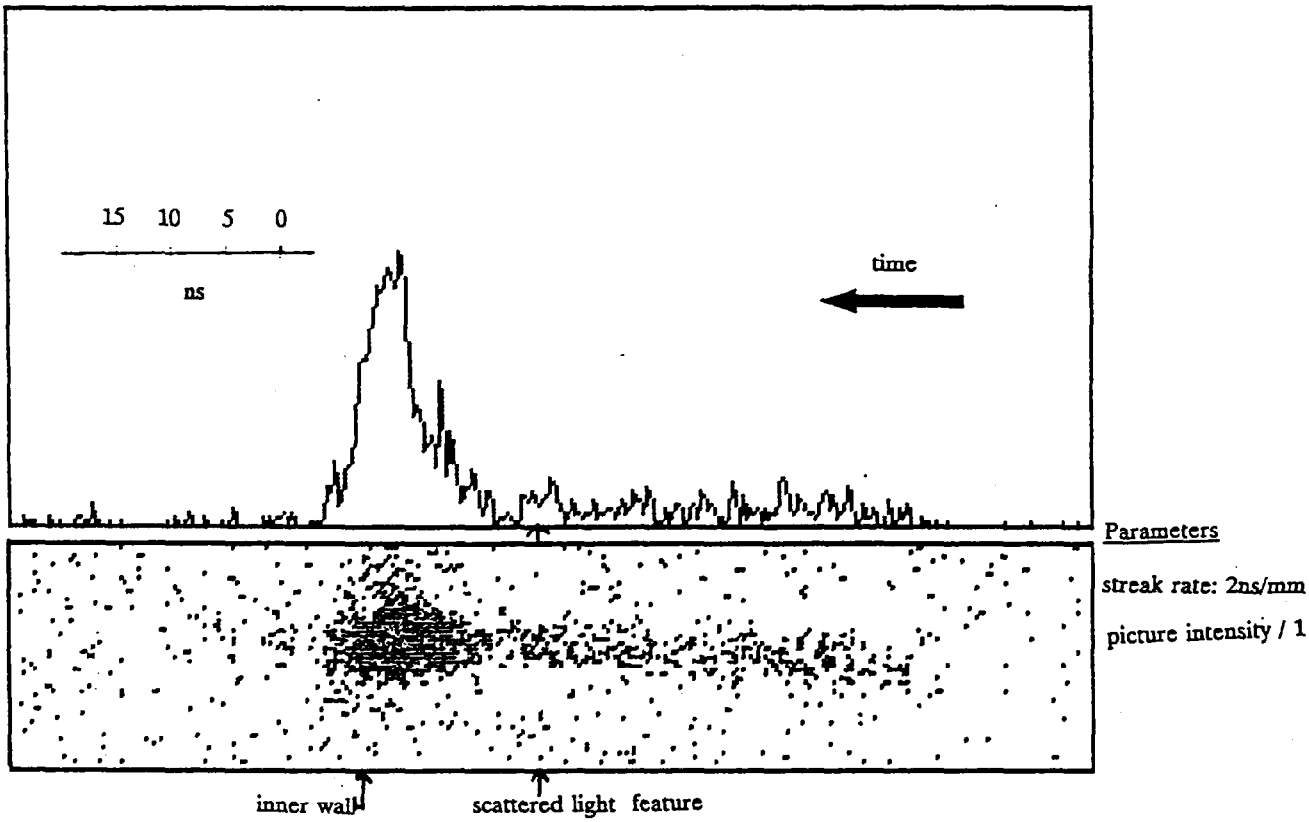

[8] Scattered signal - indicated streak rate 2ns/mm

Fig.(9) Transmission characteristics of 3 channels

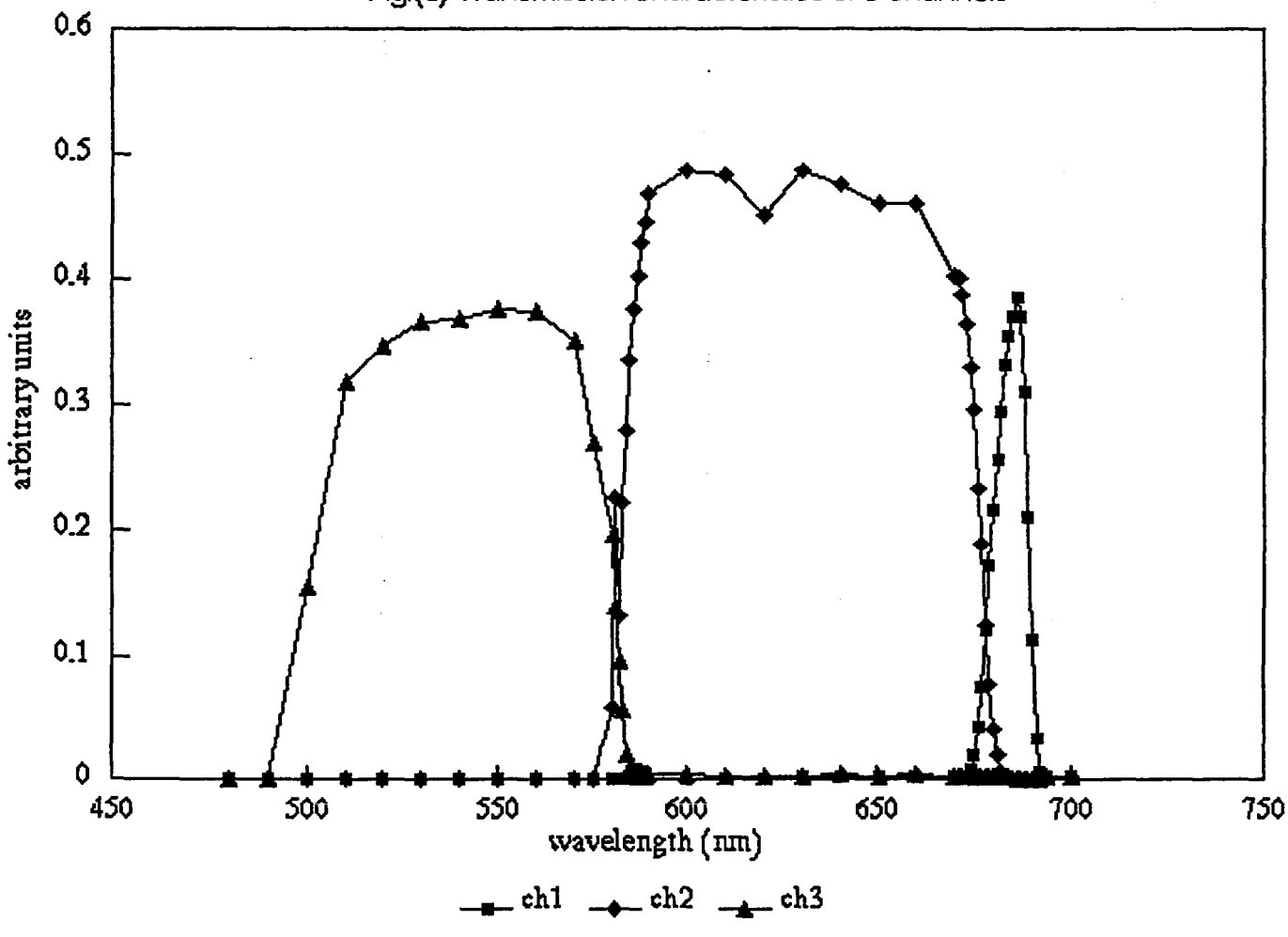

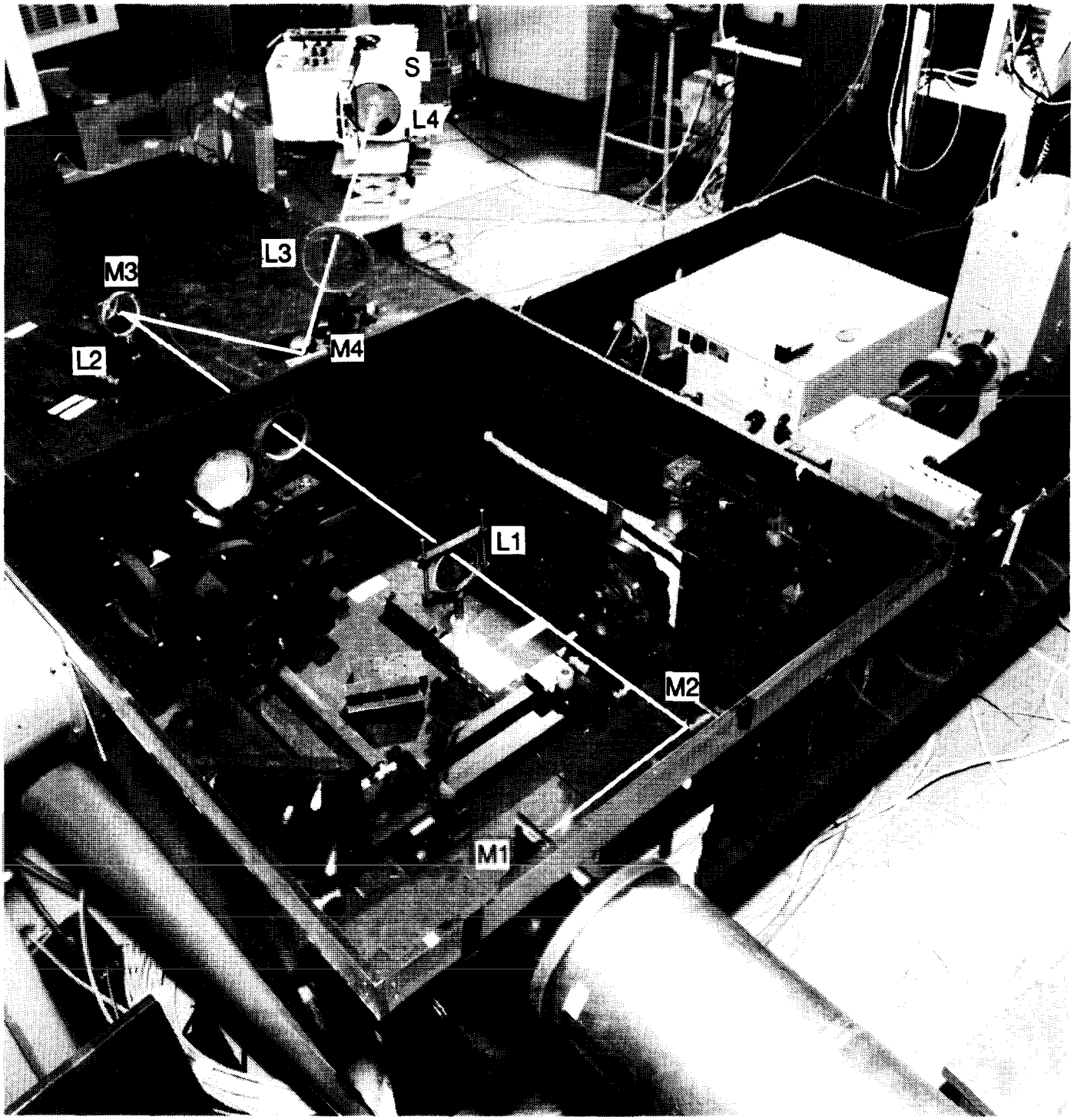

Key:

M1 - mirror 1 M2 - mirror 2 M3 - mirror 3 M4 - mirror 4
L1 - f = 0.5m lens L2 - f = 1m lens L3 - f = 0.5m lens
L4 - aspheric condenser S - streak camera - beam path

[3] The preliminary system

Fig. 4) Stray Light + Background

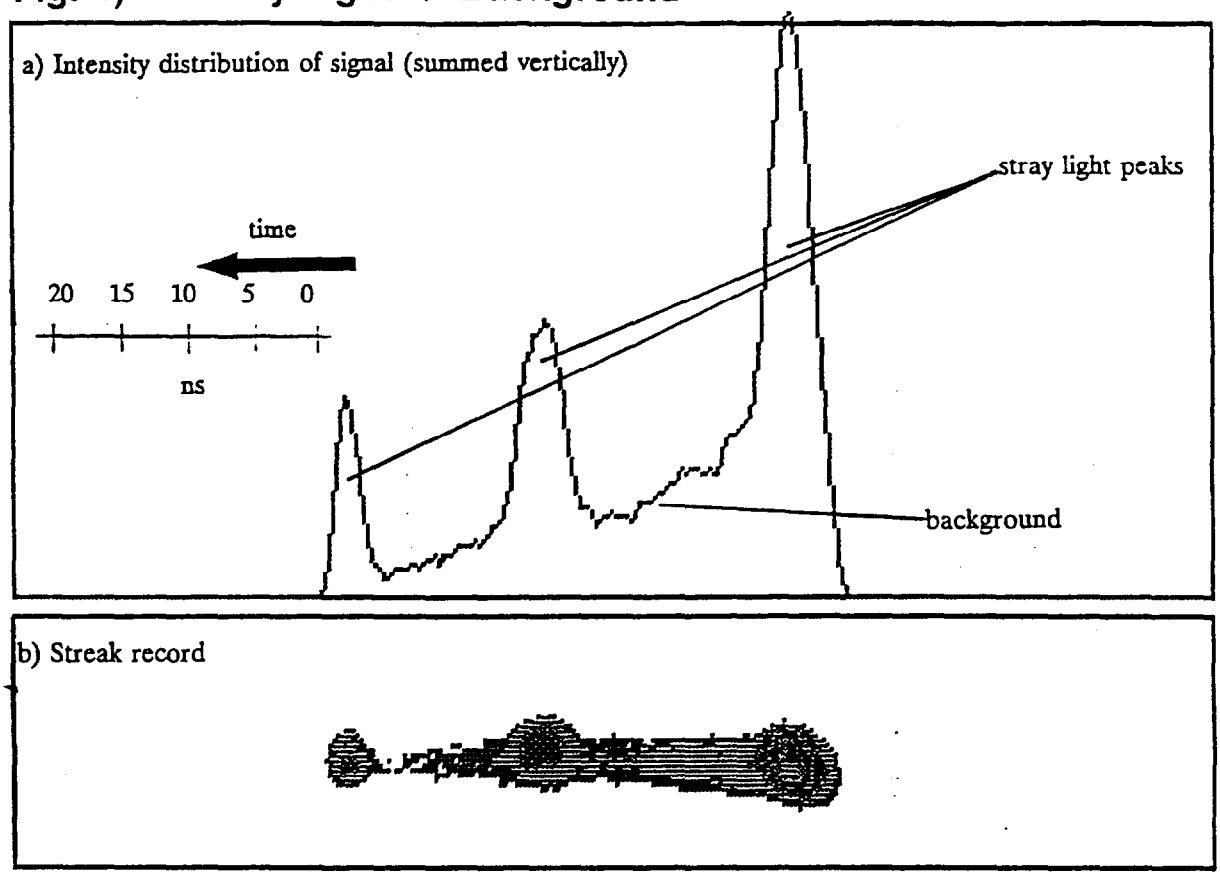

[4] First results - stray light plus background

Fig. 5) Relevant Stray Light Pulses

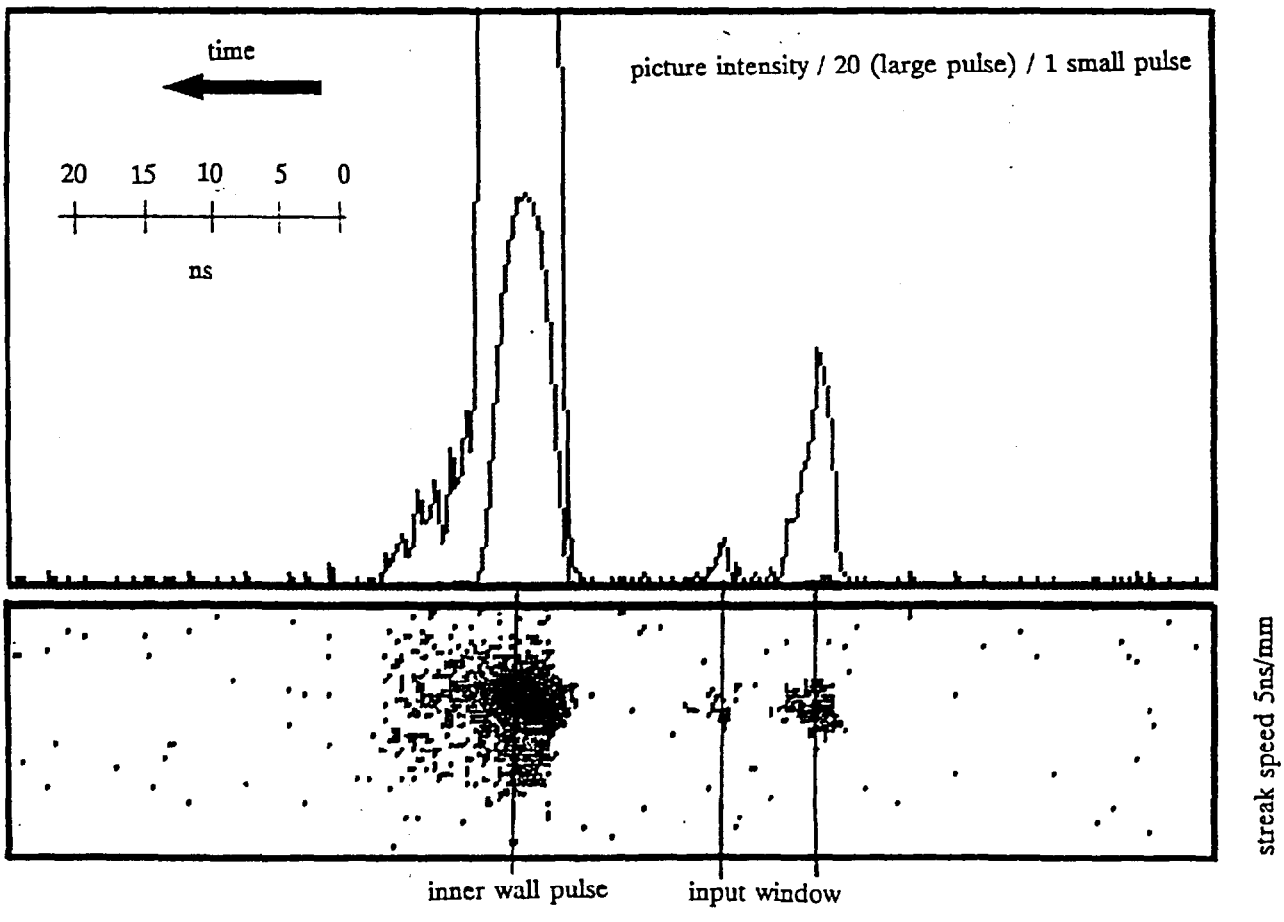

[5] Stray light signature in time window of interest

Appendix I

THE JET TEAM

JET Joint Undertaking, Abingdon, Oxon, OX14 3EA, U.K.

J.M. Adams[1], H. Altmann, A. Andersen[14], P. Andrew[18], M. Angelone[29], S.A. Arshad, W. Bailey, P. Ballantyne, B. Balet, P. Barabaschi, R. Barnsley[2], M. Baronian, D.V. Bartlett, A.C. Bell, I. Benfatto[5], G. Benali, H. Bergsaker[11], P. Bertoldi, E. Bertolini, V. Bhatnagar, A.J. Bickley, H. Bindslev[14], T. Bonicelli, S.J. Booth, G. Bosia, M. Botman, D. Boucher, P. Boucquey, P. Breger, H. Brelen, H. Brinkschulte, T. Brown, M. Brusati, T. Budd, M. Bures, T. Businaro, P. Butcher, H. Buttgereit, C. Caldwell-Nichols, D.J. Campbell, P. Card, G. Celentano, C.D. Challis, A.V.Chankin[23], D. Chiron, J. Christiansen, C. Christodoulopoulos, P. Chuilon, R. Claesen, S. Clement, E. Clipsham, J.P. Coad, M. Cornelskey[4], S. Conroy, M. Cooke, S. Cooper, J.G. Cordey, W. Core, G. Corrigan, S. Corti, A.E. Costley, G. Cottrell, M. Cox[7], P. Cripwell, H. de Blank[15], H. de Esch, L. de Kock, E. Deksnis, G.B. Denne-Hinnov, G. Deschamps, K.J. Dietz, S.L. Dmitrenko, J. Dobbing, N. Dolgetta, S.E. Dorling, P.G. Doyle, D.F. Düchs, H. Duquenoy, A. Edwards, J. Ehrenberg, A. Ekedahl, T. Elevant[11], S.K. Erents[7], L.G. Eriksson, H. Fajemirokun[12], H. Falter, D. Flory, J. Freiling[15], C. Froger, P. Froissard, K. Fullard, M. Gadeberg, A. Galetsas, D. Gambier, M. Garribba, P. Gaze, R. Giannella, A. Gibson, R.D. Gill, A. Girard, A. Gondhalekar, C. Gormezano, N.A. Gottardi, C. Gowers, B.J. Green, R. Haange, G Haas, A. Haigh, G. Hammett[6], C.J. Hancock, P.J. Harbour, N.C. Hawkes[7], P. Haynes[7], J.L. Hemmerich, T. Hender[7], F.B. Herzog, R.F. Herzog, J. Hoekzema, J. How, M. Huart, L Hughes, T.P. Hughes[4], M. Hugon, M. Huguet, A. Hwang[7], B. Ingram, M. Irving, J. Jacquinot, H. Jaeckel, J.F. Jaeger, G. Janeschitz[13], S. Jankowicz[22], O.N. Jarvis, F. Jensen, E.M. Jones, L.P.D.F. Jones, T.T.C. Jones, J-F. Junger, E. Junique, A. Kaye, B.E. Keen, M. Keilhacker, G.J. Kelly, W. Kerner, R. Konig, A. Konstantellos, M. Kovanen[20], G. Kramer[15], P. Kupschus, R. Lässer, J.R. Last, B. Laundy, L. Lauro-Taroni, K. Lawson[7], M. Lennholm, A. Loarte, R. Lobel, P. Lomas, M. Loughlin, C. Lowry, B. Macklin, G. Maddison[7], G. Magyar, W. Mandl[13], V. Marchese, F. Marcus, J. Mart, E. Martin, R. Martin-Solis[8], P. Massmann, G. McCracken[7], P. Meriguet, P. Miele, S.F. Mills, P. Millward, R. Mohanti[17], P.L. Mondino, A. Montvai[3], S. Moriyama[28], P. Morgan, H. Morsi, G. Murphy, M. Mynarends, R. Myrnäs[16], C. Nardone, F. Nave[21], G. Newbert, M. Newman, P. Nielsen, P. Noll, W. Obert, D. O'Brien, J. O'Rourke, R. Ostrom, M. Ottaviani, M. Pain, F. Paoletti, S. Papastergiou, D. Pasini, A. Peacock, N. Peacock[7], D. Pearson[12], R. Pepe de Silva, G. Perinic, C. Perry, M. Pick, R. Pitts[7], J. Plancoulaine, J-P. Poffé, F. Porcelli, L. Porte[19], R. Prentice, S. Puppin, S. Putvinsko[23], G. Radford[9], T. Raimondi, M.C. Ramos de Andrade, P-H. Rebut, R. Reichle, E. Righi, F. Rimini, D. Robinson[7], A. Rolfe, R.T. Ross, L. Rossi, R. Russ, P. Rutter, H.C. Sack, G. Sadler, G. Saibene, J.L. Salanave, G. Sanazzaro, A. Santagiustina, R. Sartori, C. Sborchia, P. Schild, M. Schmid, G. Schmidt[6], B. Schunke, S.M. Scott, A. Sibley, R. Simonini, A.C.C. Sips, P. Smeulders, R. Stankiewicz[27], M. Stamp, P. Stangeby[18], D.F. Start, C.A. Steed, D. Stork, P.E. Stott, T.E. Stringer, P. Stubberfield, D. Summers, H. Summers[19], L. Svensson, J.A. Tagle[21], A. Tanga, A. Taroni, A. Tesini, P.R. Thomas, E. Thompson, K. Thomsen, J.M. Todd, P. Trevalion, B. Tubbing, F. Tibone, E. Usselmann, H. van der Beken, G. Vlases, M. von Hellermann, T. Wade, C. Walker, R. Walton[6], D. Ward, M.L. Watkins, M.J. Watson, S. Weber[10], J. Wesson, T.J. Wijnands, J. Wilks, D. Wilson, T. Winkel, R. Wolf, B. Wolle[24], D. Wong, C. Woodward, Y. Wu[25], M. Wykes, I.D. Young, L. Zannelli, Y. Zhu[26], W. Zwingmann.

PERMANENT ADDRESSES

1. UKAEA, Harwell, Didcot, Oxon, UK.
2. University of Leicester, Leicester, UK.
3. Central Research Institute for Physics, Academy of Sciences, Budapest, Hungary.
4. University of Essex, Colchester, UK.
5. ENEA-CNR, Padova, Italy.
6. Princeton Plasma Physics Laboratory, New Jersey, USA.
7. UKAEA Culham Laboratory, Abingdon, Oxon, UK.
8. Universidad Complutense de Madrid, Spain.
9. Institute of Mathematics, University of Oxford, UK.
10. Freien Universität, Berlin, F.R.G.
11. Swedish Energy Research Commission, S-10072 Stockholm, Sweden.
12. Imperial College of Science and Technology, University of London, UK.
13. Max Planck Institut für Plasmaphysik, Garching bei München, FRG.
14. Risø National Laboratory, Denmark.
15. FOM Instituut voor Plasmafysica, 3430 Be Nieuwegein, The Netherlands.
16. University of Lund, Sweden.
17. North Carolina State University, Raleigh, NC, USA
18. Institute for Aerospace Studies, University of Toronto, Downsview, Ontario, Canada.
19. University of Strathclyde, 107 Rottenrow, Glasgow, UK.
20. Nuclear Engineering Laboratory, Lapeenranta University, Finland.
21. CIEMAT, Madrid, Spain.
22. Institute for Nuclear Studies, Otwock-Swierk, Poland.
23. Kurchatov Institute of Atomic Energy, Moscow, USSR
24. University of Heidelberg, Heidelberg, FRG.
25. Institute for Mechanics, Academia Sinica, Beijing, P.R. China.
26. Southwestern University of Physics, Leshan, P.R. China.
27. RCC Cyfronet, Otwock Swierk, Poland.
28. JAERI, Naka Fusion Research Establishment, Ibaraki, Japan.
29. ENEA, Frascati, Italy.

At 1st June 1991